On the long-term migration of uranyl in bentonite barrier for high-level radioactive waste repositories: the effect of different host rocks

Xiaoyuan Cao [1], Liange Zheng [2]*, Deyi Hou [1] and Litang Hu [3,4]

1 School of Environment, Tsinghua University, Beijing 100084, China;
2 Energy Geosciences Division, Lawrence Berkeley National Laboratory, 1 Cyclotron Rd Berkeley, CA, USA;
3 College of Water Sciences, Beijing Normal University, Beijing 100875, China;
4 Engineering Research Center of Groundwater Pollution Control and Remediation of Ministry of Education, Beijing Normal University, Beijing 100875, China
* Correspondence: lzheng@lbl.gov; Tel.: 1-510-486-5502

ABSTRACT:

Repositories for high level radioactive waste hosted in argillite or granite with bentonite backfill are the two disposal concepts that been extensively studied. A general perception is that granite has very low sorption capacity and therefore is disadvantageous in retarding the migration of radionuclides in comparison with argillite. However, when there is bentonite backfill, does the sorption capacity of granite really matter for the migration of radionuclides? How different host rocks would affect the migration of U(VI) through the bentonite backfill of an engineered barrier system (EBS), and which properties of the host rocks cause those differences in migration, given that migration of radionuclides is a critical measure in assessing the performance of a repository? Here we present two coupled thermal, hydrological, and chemical models for the transport of U(VI), each with an identical setup except for the type of host rock (argillite vs granite rock).

Comparisons between our models show that the different host rocks exert their influence on migration of U(VI) via regulating the chemical conditions in the bentonite, which affect the concentration of U(VI) at the source and the adsorption of U(VI) in the bentonite. The key chemical conditions are pH, Ca^{+}, and HCO_3^{-} concentration in pore-water, which are strongly affected by soluble carbonate minerals. Our models also show the occurrence of illitization (dissolution of smectite and precipitation of illite) in the bentonite, which affects the migration of U(VI) through changing pH and the quantity of adsorbents. Although generalization of current model results for granite and argillite should be done carefully, the simulations highlight the importance of pore-water chemistry in host rock, as well as bentonite-host rock interactions, when assessing the

performance of a repository. In comparison to properties such as thermal conductivity, permeability, and adsorption capacity, properties that have been studied intensively, the pore-water chemistry of host rocks deserve equal or even more attention because of its strong influence on radionuclide migration.

1. Introduction

Multi-barrier nuclear waste repository isolation systems within the deep subsurface are under consideration throughout the world to isolate high-level radioactive waste from the biosphere. These systems typically involve both a natural barrier system, which includes the repository host rock and surrounding subsurface environment, and an engineered barrier system (EBS), which includes waste canisters, a buffer (or backfill) and/or a concrete liner. Currently, argillite and crystalline rock are the two types of host rock that have been most extensively studied.

Crystalline rocks/granite formations have been considered as a host rock throughout the world (e.g., Korea, Japan, China) and are being studied at several underground research laboratories—for example., in the Fennoscandian Shield, Sweden (Martin and Christiansson, 2009), at the Grimsel Test Site, Switzerland (Hadermann and Heer, 1996), and in the Beishan area, China (Cao et al., 2017b). The most advantageous features for crystalline/granite rock with respect to radioactive waste isolation include mechanical stability, low permeability (without fractures), high thermal conductivity, and widespread geologic occurrence.

Clay/shale/argillite is also a subject of widespread interest as a potential host rock for radioactive waste disposal. This type of rock is of interest because of its low permeability, low diffusion coefficient, high retention capacity for radionuclides, its ability to self-seal fractures induced by tunnel excavation, and the widespread geologic prevalence of this rock type (Bianchi et al., 2013; Hansen et al., 2010). The predominance of diffusive transport and adsorption in clay media are key attributes that make clay rock formations target sites for disposal of high-level radioactive waste. Extensive scientific knowledge has been obtained to assess the long-term argillite repository isolation performance of nuclear waste, especially through studies at underground research laboratories such as Callovo-Oxfordian argillites at Bure, France (Fouché et al., 2004), Toarcian argillites at Tournemire, France (Patriarche et al., 2004), Opalinus Clay at Mont Terri, Switzerland (Meier et al., 2000),

and Boom clay at the Mol, Belgium (Barnichon and Volckaert, 2003).

The selection of repository host rock is a very complex process, affected by both technical and nontechnical factors. In terms of technical feasibility, crystalline/granite and argillite both have advantages and disadvantages. When weighting the technical features of these potential host rocks, the EBS (usually backfilled with bentonite] must also be taken into account, because the interaction between the EBS and host rock is very important for the performance of the repository (Zheng et al., 2015). Bentonite is a clay consisting mostly of smectite (montmorillonite) along with small amounts of other minerals such as quartz and feldspar. In some disposal concepts (e.g., Huertas et al., 2000; SKB, 2006)), the backfill contains exclusively bentonite, but in some concepts (JNC, 1999) backfills are mixtures of bentonite and graphite or silica phases (e.g., quartz) to enhance thermal conductivity. For repository buffer materials, the key requirements are low hydraulic conductivity, self-sealing ability, and durability of the properties over the very long term (Vomvoris et al., 2015). The primary safety functions of bentonite barriers include limiting transport in the near field, reducing microbial activity, damping rock-shear movements, resisting mineralogical transformations, preventing canister sinking, and limiting pressure on canister and rock (Vomvoris et al., 2015).

Evaluating the performance of a repository is extremely complex. It involves studying the evolution of multiple components, including waste form, waste package, EBS, and host rocks and biosphere. Each of these components is affected by coupled thermal, hydrological, mechanical, and chemical (THMC) processes (and these processes have to be studied at different scales), and ultimately the interactions between components have to be evaluated in an integrated way. Regarding crystalline and argillite repositories, extensive studies have been conducted to shed light on various aspects using laboratory experiments, large-scale tests at underground laboratories, and numerical models. Some studies have focused on thermal evolution in the repository—for example, Greenberg et al. (2013) evaluated thermal evolution in an argillite repository using semi-analytical solutions, while Hardin et al. (2015) studied the thermal aspect of various host rocks including salt, argillite, and crystalline. Some studies have focused on large-scale hydrological behavior, such as modeling groundwater transport around a deep borehole nuclear waste repository in crystalline bedrock (Lubchenko et al., 2015); others have focused on the hydraulic connection between an emplacement drift and

surrounding hydrogeological units near a repository in argillite bedrock (Bianchi et al., 2015). Coupled THM (e.g. Chen et al., 2009; Gens et al., 2009; Sánchez et al., 2012), THC (Zheng et al., 2011) and THMC (Zheng and Samper, 2008; Gens et al., 2010; Rutqvist et al., 2014; Zheng et al., 2014; 2015) processes in EBS bentonite in crystalline and argillite have been extensively studied using numerical models and *in situ* tests.

Last but not least, the migration of radionuclides in an EBS and host rock has been the focus of numerous studies. Voutilainen et al. (2017) simulated transport of cesium in Grimsel granodiorite with micrometer-scale heterogeneities; they concluded that the heterogeneity of the mineral structure at the micrometer scale could significantly affect the diffusion and adsorption of cesium in Grimsel granodiorite at the centimeter scale. Jin et al. (2016) conducted a surface complexation modeling of U(VI) adsorption, using a Generalized Composite model on granite at ambient/elevated temperature; model results showed that the exchange reaction is not important for U(VI) adsorption on granite.

All these studies have deepened our understanding of the processes that control the transport of radioactive waste in the host rock and have equipped us with increasingly better tools to assess the performance of a repository in either crystalline or argillite. Here, our focus is on radionuclide migration, one of the ultimate measures of repository performance. A general perception is that granite has very low sorption capacity and therefore disadvantageous in retarding the migration of radionuclides in comparison with argillite. However, when there is bentonite backfill, does the sorption capacity of granite really matter for the migration of radionuclides? The question we are trying to address is, assuming they have the same EBS, how do different host rocks (argillite vs granite) affect the migration of radionuclides (e.g. uranyl or U(VI)), and which host-rock properties cause the difference? In this paper, we present coupled THC models for transport of U(VI) that have identical setup except for the type of host rock (argillite vs granite rock). One model (called Case_G) assumes that the host rock has the properties of granite from Beishan, China (Cao et al., 2017a), and the other (called Case_A) assumes that the host rock has the properties of Opalinus Clay (Bossart, 2011; Lauber et al., 2000). The paper starts with a description of the conceptual model, then presents the details of the numerical model and a discussion of model results, and finally makes some concluding remarks.

2. Model Development

2.1. Conceptual model

When designing a numerical model to explore the impact of different host rocks on the migration of radionuclides, we first need to decide what processes need to be taken into account in the model. Due to the heat emission from HLW, heat convection and conduction are apparently indispensible processes in the model. Regarding water flow in the bentonite barrier and host rock, because of the importance of vapor diffusion (Ho and Webb, 1996; Zheng et al., 2016) during the early unsaturated stage, we consider two-phase (gas and liquid) flow in the model, with a gas phase including vapor and an air and liquid phase including water and dissolved air.

Uranium, in particular the isotopes ^{238}U (half-life, $t_{1/2}=4.468\times10^{9}$ a) and ^{235}U ($t_{1/2}=7.038\times10^{8}$ a), represents the main fraction of spent nuclear fuel rods (about 95%) (Joseph et al., 2017) and, consequently, constitutes the majority of HLW. It accounts for only 0.005% of the initial total radiotoxicity of the spent nuclear fuel (OECD, 2006). However, after about one million years, owing to the decay of plutonium and minor actinides, the uranium contribution to the total radiotoxicity increases to about 30%. Moreover, the chemotoxicity of ^{238}U is about two orders of magnitude larger than its radiotoxicity (Burkart et al., 2005). In general, uranium is stored in the oxidation state IV in the form of UO_2, which is insoluble and immobile under most repository-relevant conditions. However, several oxidation processes can occur whereby U(IV) can be partly transformed to U(VI) (Bruno et al., 2004; Baeyens et al., 2014), resulting in more mobile species. Therefore, our model focuses on the migration of U(VI).

Experimental and modeling studies have been conducted to investigate different aspects of U(VI) migration, including the adsorption of U(VI) (Boult et al., 1998; Majdan et al., 2010; Missana et al., 2004, Gao et al., 2017), ion exchange processes (Chung et al., 2013; Reinoso-Maset and Ly, 2016), and the effects of particle size, pH value, and the concentration of uranium and temperature on the migration of U(VI) in groundwater (Wei, 2012). Adsorption/desorption is an important reaction controlling the migration of U(VI) in bentonite and has been widely studied. Although there are still some reactive transport models utilizing the distribution coefficient (constant-Kd) approach to describe the retardation of U(VI) in aquifers caused by adsorptions (Bethke and

Brady, 2010), surface complexation models are currently more widely used for calculating the adsorption/desorption of U(VI). Typically, surface complexation reactions are derived by fitting the macroscopic dependence of adsorption on pH (Davis et al., 1998). Surface reactions can be coupled with aqueous complexation reactions to simulate macroscopic adsorption as a function of aqueous chemical conditions. Numerous surface complexation models have been developed to describe the sorption of uranium on clay minerals; these models differ in the types of sites, their ways of accounting for the electrostatic term, and the surface species (i.e., surface complexation binding of U(VI)).

In this study, we use a two-site protolysis non-electrostatic surface complexation and cation exchange sorption model (2 SPNE SC/CE) (Bradbury and Baeyens, 2011). In this model, surface protonation reactions that involve a strong site and two weak sites are used to describe acid-base titration measurements, whereas surface complexation reactions with the one strong site and two weak sites are needed to describe the sorption edge and isotherm measurements for the sorption of U(VI) on smectite and illite. A detailed discussion of the 2 SPNE SC/CE model for smectite was given in Bradbury and Baeyens (2005); a similar discussion for illite was given in Bradbury and Baeyens (2009a; 2009b). The first twelve reactions listed in Table 1 are the surface protonation reactions on montmorillonite (smectite) and illite (Bradbury and Baeyens, 2009b), the next six reactions are the surface complexation reactions for the sorption of U(VI) on illite, and the last six reactions are the surface complexation reactions for the sorption of U(VI) on montmorillonite (smectite). Table 2. shows the cation exchange reactions on montmorillonite (smectite).

Table 1. The surface protonation reactions on montmorillonite (smectite) and illite and surface complexation reactions for the sorption of U(VI) on montmorillonite (smectite) and illite

Surface complexation	Log K
ill_sOH$_2^+$ = ill_sOH + H$^+$	-4
ill_sO$^-$ + H$^+$ = ill_sOH	6.2
ill_w1OH$_2^+$ = ill_w1OH+ H$^+$	-4
ill_w1O$^-$ + H$^+$ = ill_w1OH	6.2
ill_w2OH$_2^+$ = ill_w2OH+ H$^+$	-8.5
ill_w2O$^-$ + H$^+$ = ill_w2OH	10.5
mon_sOH$_2^+$ = mon_sOH + H$^+$	-4.5
mon_sO$^-$ + H$^+$ = mon_sOH	7.9
mon_w1OH$_2^+$ = mon_w1OH+ H$^+$	-4.5
mon_w1O$^-$ + H$^+$ = mon_w1OH	7.9
mon_w2OH$_2^+$ = mon_w2OH+ H$^+$	-6
mon_w2O$^-$ + H$^+$ = mon_w2OH	10.5
ill_sOUO$_2^+$ + H$^+$= ill_sOH + UO$_2^{+2}$	-2
ill_sOUO$_2$OH+ 2H$^+$ = ill_sOH + UO$_2^{+2}$+H$_2$O	3.5
ill_sOUO$_2$(OH)$_2^-$+3H$^+$=ill_sOH + UO$_2^{+2}$+2H$_2$O	10.6
ill_sOUO$_2$(OH)$_3^-$+ 4H$^+$ = ill_sOH + UO$_2^{+2}$+3H$_2$O	19
ill_w1OUO$_2^+$ +H$^+$= ill_w1OH+ UO$_2^{+2}$	-0.1
ill_ w1OUO$_2$OH+2H$^+$ = ill_w1OH+ UO$_2^{+2}$+H$_2$O	5.3
mon_sOUO$_2^+$ + H$^+$= mon_sOH + UO$_2^{+2}$	-3.1
mon_sOUO$_2$OH+ 2H$^+$ = mon_sOH + UO$_2^{+2}$+H$_2$O	3.4
mon_sOUO$_2$(OH)$_2^-$+3H$^+$=mon_sOH + UO$_2^{+2}$+2H$_2$O	11
mon_sOUO$_2$(OH)$_3^-$+ 4H$^+$ = mon_sOH + UO$_2^{+2}$+3H$_2$O	20.5
mon_w1OUO$_2^+$ +H$^+$= mon_w1OH+ UO$_2^{+2}$	-0.7
mon_w1OUO$_2$OH+2H$^+$ = mon_w1OH+ UO$_2^{+2}$+H$_2$O	5.7

Table 2. Cation exchange reactions on montmorillonite (smectite)

Cation exchange reaction	$K_{Na/M}$
Na$^+$ + mon-H = mon-Na + H$^+$	1
Na$^+$ + mon-K = mon-Na + K$^+$	0.2
Na$^+$ + 0.5 mon-Ca = mon-Na + 0.5 Ca^{+2}	0.4
Na$^+$ + 0.5 mon-Mg = mon-Na + 0.5 Mg^{+2}	0.45
Na$^+$ + 0.5 mon-UO$_2^{+2}$ = mon-Na + 0.5 UO$_2^{+2}$	0.84

Aqueous complexes considered in this study are listed in Table 3, which were selected based on speciation modeling using EQ3/6 and database data0.ymp.R5. Reaction constants are taken from Spycher

et al (2011), most of which are largely consistent with those used in Davis et al. (2004). Our speciation calculation is consistent with other studies (Dong et al., 2006; Fox et al., 2006; Stewart et al., 2010, Tournassat et al., 2018) that the dominant ones are $Ca_2UO_2(CO_3)_3$ and $CaUO_2(CO_3)_3^{-2}$. A chemical model that neglects these two species could significantly underestimate the total aqueous concentration of U (VI).

Table 3. Aqueous complexes for U(VI)

Aqueous complexes	Reactions								Logk(25 ℃)
	Stoi	Species	Stoi	Species	Stoi	Species	Stoi	Species	
$(UO_2)_{11}(CO_3)_6(OH)_{12}^{-2}$	-18	H^+	6	HCO_3^-	11	UO_2^{+2}	12	H_2O	25.855
$(UO_2)_2(OH)_2^{+2}$	-2	H^+	2	H_2O	2	UO_2^{+2}			5.659
$(UO_2)_2CO_3(OH)_3^-$	-4	H^+	1	HCO_3^-	2	UO_2^{+2}	3	H_2O	11.245
$(UO_2)_2OH^{+3}$	-1	H^+	1	H_2O	2	UO_2^{+2}			2.729
$(UO_2)_3(CO_3)_6^{-6}$	-6	H^+	3	UO_2^{+2}	6	HCO_3^-			8.099
$(UO_2)_3(OH)_4^{+2}$	-4	H^+	3	UO_2^{+2}	4	H_2O			11.962
$(UO_2)_3(OH)_5^+$	-5	H^+	3	UO_2^{+2}	5	H_2O			15.624
$(UO_2)_3(OH)_7^-$	-7	H^+	3	UO_2^{+2}	7	H_2O			32.2
$(UO_2)_3O(OH)_2(HCO_3)^+$	-4	H^+	1	HCO_3^-	3	H_2O	3	UO_2^{+2}	9.746
$(UO_2)_4(OH)_7^+$	-7	H^+	4	UO_2^{+2}	7	H_2O			21.995
$UO_2(SO_4)_2^{-2}$	1	UO_2^{+2}	2	SO_4^{-2}					-3.962
UO_2Cl^+	1	Cl^-	1	UO_2^{+2}					-0.141
$UO_2Cl_2(aq)$	1	UO_2^{+2}	2	Cl^-					1.146
UO_2F^+	1	F^-	1	UO_2^{+2}					-5.034
$UO_2F_2(aq)$	1	UO_2^{+2}	2	F^-					-8.519
$UO_2F_3^-$	1	UO_2^{+2}	3	F^-					-10.762
$UO_2F_4^{-2}$	-1	UO_2^{+2}	4	F^-					-11.521
$UO_2OSi(OH)_3^+$	1	H^+	1	$SiO_2(aq)$	1	UO_2^{+2}	2	H_2O	2.481
$UO_2SO_4(aq)$	-1	SO_4^{-2}	1	UO_2^{+2}					-3.049
UO_2OH^+	-2	H^+	1	H_2O	1	UO_2^{+2}			5.218
$UO_2(OH)_2(aq)$	-4	H^+	2	H_2O	1	UO_2^{+2}			12.152
$UO_2(OH)_4^{-2}$	-1	H^+	1	UO_2^{+2}	4	H_2O			32.393
$UO_2CO_3(aq)$	-2	H^+	1	HCO_3^-	1	UO_2^{+2}			0.396
$UO_2(CO_3)_2^{-2}$	-3	H^+	2	HCO_3^-	1	UO_2^{+2}			4.048
$UO_2(CO_3)_3^{-4}$	-3	H^+	3	HCO_3^-	1	UO_2^{+2}			9.141
$CaUO_2(CO_3)_3^{-2}$	-3	H^+	1	Ca^{+2}	3	HCO_3^-	1	UO_2^{+2}	3.806
$Ca_2UO_2(CO_3)_3$	-3	H^+	2	Ca^{+2}	3	HCO_3^-	1	UO_2^{+2}	0.286

In the geological repository environment, radionuclides originate from used-fuel waste packages. The degradation of these waste packages is an extremely complex issue. Used fuel pellets are largely composed of solid UO_2, which would usually undergo oxidative dissolution with oxidants (typically H_2O_2) produced by α-radiolysis (De Windt et al., 2006):

$$UO_2(s) + H_2O_2 = UO_2^{+2} + 2OH^- \quad (1)$$

U(VI) (as UO_2^{+2}) is produced and would precipitate as a secondary U(VI) phase. For example, in a 10-year degradation of UO_2(s) by dripping water (Bernot, 2005), 11 phases were identified, including schoepite, soddyite, boltwoodite or na-boltwoodite, and uranophane. The formation of these phases depends on possible environmental conditions, such as the aqueous and mineralogical composition of the media in contact with the waste package, as well as the pH, Eh, and CO_2 partial pressure. The oxidation of UO_2(s) and the formation of secondary U(VI) phases are slow and usually simulated as kinetic processes (De Windt et al., 2003). However, as the waste packages degrade, the U concentration is controlled by the least soluble uranium phase that is stable under the given geochemical conditions. To be conservative, and for reasons of simplicity, the source concentration of uranium is usually determined by the solubility of the U(VI) phase that is possibly present in the given performance assessment environment. After an evaluation of the possible U(VI) minerals, Bernot (2005) selected schoepite as the controlling phase, because the laboratory studies of Wronkiewicz et al. (1996) showed it to be the dominant early-formed phase in UO_2(s) degradation. In this paper, we take the same strategy and assume that the waste package is composed only of schoepite; the concentration of U(VI) is then controlled by the following reaction:

$$\text{Schoepite} + 2H^+ = 3H_2O + UO_2^{+2} \quad \log K(25\ ^oC) = 4.844 \qquad (2)$$

The logK value of the reaction is taken from the EQ3/6 database data0.ymp.R5, and the variation in logK as a function of temperature is given as:

$$\text{LogK}(T) = 14.6\ln(T) - 92.016 - 1.644\times10^{-2}T + 5.5357\times10^{-3}/T \qquad (3)$$

where T is temperature (K).

In addition to the chemical reactions associated with U(VI) and aqueous complexation, mineral dissolution/precipitation for major ions are also needed to be accounted for (see next section for details), because it determines the chemical environment under which U(VI) migrates.

It is known that chemical reactions are mostly temperature dependent. In this paper, effect of temperature on reaction constants for aqueous complexation and mineral dissolution/precipitation are considered via temperature dependent logK (see Equation (3)). However, reaction constants for cation exchange and surface complexation were seldom measured for

more than one temperature point, we therefore in the paper did not consider the effect of temperature on cation exchange and surface complexation.

2.2. Numerical model

Our modeling work is more of an exploratory study rather than associated with any real HLW repository, with the choice of properties for the EBS bentonite and host rock largely determined by data availability. As mentioned above, we developed two cases for comparison: Case_A and Case_G have identical setup except for the host rock: Case_A has argillite host rock; Case_G has granite host rock. EBS bentonite has the properties of FEBEX bentonite, which has been extensively characterized by laboratory and field experiment (Huertas et al., 2000) and studied by modeling work (Zheng and Samper, 2008; Zheng et al., 2011). For Case_A, the properties of argillite host rock are the same as Opalinus Clay (Bossart, 2011; Lauber et al., 2000). For Case_G, the properties of granite host rock are taken from granites at Beishan, China, a potential repository site that is in an arid region in northwestern China. It is mainly composed of weathered granites with different periods of crystalline rocks.

2.2.1. Model domains

Our model considers two material zones for the bentonite and host rock (granite or argillite). Bentonite is located within 0.45 m ~ 1.135 m, with the remaining domain up to 50 m used to simulate the host rock. The model simulation was conducted in a nonisothermal mode with a time-dependent heat power input (Rutqvist et al., 2014). The power curve was adopted from representative heating data from the U.S. DOE's Used Fuel Disposition campaign for pressurized water reactor (PWR) used fuel (Rutqvist et al., 2014). The initial temperature is uniform and equal to 12ºC. Initially the EBS bentonite has a water saturation of 59% and a suction of 1.11×10^5 kPa. The host rock is fully saturated. Boundary conditions for flow include: (1) no flow at r (radius) = 0.45 m and (2) a prescribed liquid pressure of 7 bars at r = 50 m. From time zero, the FEBEX bentonite simultaneously undergoes resaturation, heating, chemical alteration, and stress changes. To illustrate the THMC changes in bentonite and host rocks changes, we mostly used the temporal evolution at four points (A, B, C, and D) located on the bentonite and host rock (Fig. 1).

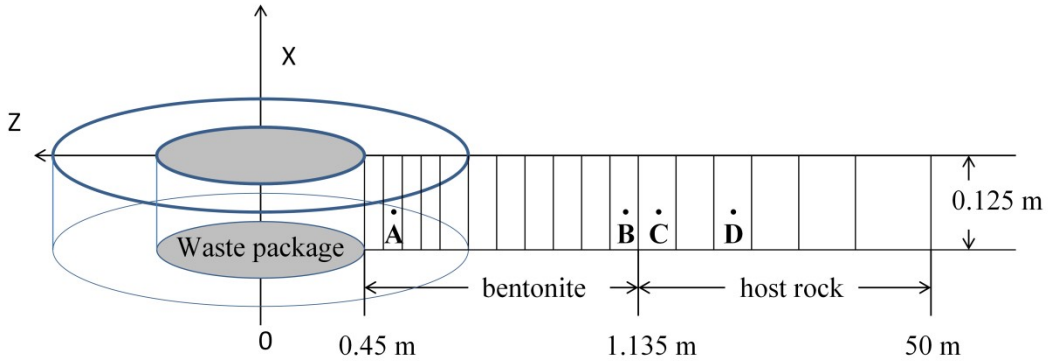

Fig. 1. Mesh used for the model, not to scale: Point A is located at r=0.479 m; B is located at r = 1.13 m in the bentonite next to the bentonite-host rock interface; C is located in host rock next to the bentonite-host rock interface with r=1.3 m, and D is 10 m away from the bentonite-host rock interface.

2.2.2. Hydrological parameters

When two-phase flow models are used to simulate the unsaturated stage in a bentonite barrier (the host rock near the bentonite barrier might go through a short desaturation phase), two key parameters are relative permeability and capillary pressure function, which are given below.

The capillary pressure (retention curve) is calculated by the van Genuchten function as:

$$P_{cap}=-\frac{1}{a}\left(\left[S^{*}\right]^{-1/m}-1\right)^{1-m} \quad (4)$$

where P_{cap} is the capillary pressure (Pa), $S^{*}=(S_l-S_{lr})/(1-S_{lr})$, S_l is the water saturation, and S_{lr} is the residual water saturation, which is 0.001 for bentonite, 0.01 for the host rock. Relative permeability has been consistently used by different models (Kuhlman and Gaus, 2014; Sánchez et al., 2012; Zheng et al., 2011), and we use the same function here:

$$k_{rl}=S_l^4 \quad (5)$$

In addition, relative permeability for host rock is calculated by the function (6):

$$K_{rl}=\begin{cases}\sqrt{S^{*}}\left\{1-\left(1-\left[S^{*}\right]^{1/\lambda}\right)^{\lambda}\right\}^2 & if \quad S_l<S_{ls}\\ 1 & if \quad S_l\geq S_{ls}\end{cases} \quad (6)$$

where$\lambda$is m in van Genuchten's notation, S_{lr} is 0.02 for argillite and 0.01for granite.

The effective permeability of bentonite has been under scrutiny by modelers (e.g. Zheng et al., 2011) because of its critical role in determining the hydration of bentonite (Table 4). The plausible saturated permeability for FEBEX bentonite in the initial state could be in a range from 1×10^{-21} to 9×10^{-21} m^2, based on various sources (Chen et al., 2009; Kuhlman and Gaus, 2014; Sánchez et al., 2012; Zheng et al., 2011), and we use 2.15×10^{-21} m^2 in the model. Meanwhile, the parameters of host rock have been verified by previous studies (Bossart, 2011; Cao et al., 2017a). Note that because current model is 1-D model and fractures cannot be considered explicitly for granite host rock, we use equivalent permeability for granite while granite is treated as porous medium.

Because thermal conductivity is a function of water saturation, we use a linear relationship implemented in TOUGH2 (Pruess et al., 1999):

$$K_{th} = K_{wet} + S_l (K_{wet} - K_{dry}) \quad (7)$$

where K_{wet} is the thermal conductivity under fully saturated conditions, K_{dry} is the thermal conductivity under dry conditions, and S_l is the liquid saturation degree.
The thermal and hydraulic parameters of bentonite, granite, and argillite are shown in Table 4.

Table 4. Thermal and hydrodynamic parameters

Parameter	Bentonite	Granite	Argillite
Grain density [kg/m^3]	2780	2650	2700
Porosity ϕ	0.41	0.001	0.15
Saturated permeability [m^2]	2.15×10^{-21}	1.0×10^{-18}	5.0×10^{-20}
Relative permeability, k_{rl}	*Eq.(5)*	*Eq.(6)*	*Eq.(6)*
Van Genuchten $1/\alpha$ [1/Pa]	1.1×10^{-8}	9.6×10^{-4}	6.8×10^{-7}
Van Genuchten m	0.60	0.492	0.595
Compressibility, β [1/Pa]	5.0×10^{-8}	3.7×10^{-10}	3.2×10^{-9}
Thermal expansion coeff. [1/°C]	1.0×10^{-4}	1.0×10^{-4}	1.0×10^{-4}
Dry specific heat [J/kg- °C]	1091	1000	900
Thermal conductivity [W/m-°C] dry/wet	0.47/1.15	3.2/3.3	3.0/3.0
Effective vapor diffusion coefficient (m^2/s)	2.03×10^{-4}	2.03×10^{-4}	2.03×10^{-4}

2.2.3. Chemical parameters

The pore-water and mineralogical composition must be known for chemical modeling. Table 5 lists the pore-water composition of

bentonite—assumed to be FEBEX bentonite (Fernández et al., 2000), and two types of host rocks: granite—assumed to be Beishan granite from Northwestern China (Cao et al., 2017b), argillite—assumed to be Opalinus Clay from Switzerland (Fernández et al., 2007). Table 6 lists the mineralogical composition of bentonite (Huertas et al., 2000), granite (Beishan granite) (Li, 2017), and argillite (Opalinus clay) (Bossart, 2011; Fernández et al., 2007; Lauber et al., 2000). The pH value for these three types of pore-waters are all slightly alkaline. The main anions and cations of the groundwater are similar among the bentonite, granite, and argillite. It shows that Cl^- and SO_4^{2-} are the main anions, and Na^+ and Mg^{+2} are the main cations. As for the mineralogical composition, bentonite is dominated by smectite, granite is mainly composed of quartz and feldspar, and argillite contains mostly illite, quartz, kaolinite and smectite.

Table 5. Pore-water composition (mol/kg water except for pH) of bentonite, granite and argillite.

	Bentonite	Granite	Argillite
pH	7.72	7.5	7.38
Cl	1.6×10^{-1}	2.63×10^{-2}	3.32×10^{-1}
SO_4^{-2}	3.2×10^{-2}	1.00×10^{-2}	1.86×10^{-2}
HCO_3^-	4.1×10^{-4}	2.34×10^{-3}	5.18×10^{-3}
Ca^{+2}	2.2×10^{-2}	1.17×10^{-3}	2.26×10^{-2}
Mg^{+2}	2.3×10^{-2}	7.43×10^{-3}	2.09×10^{-2}
Na^+	1.3×10^{-1}	3.63×10^{-2}	2.76×10^{-1}
K^+	1.7×10^{-3}	3.85×10^{-4}	2.16×10^{-3}
Fe^{+2}	2.06×10^{-8}	2.06×10^{-8}	3.45×10^{-6}
SiO_2(aq)	1.1×10^{-4}	1.91×10^{-4}	1.10×10^{-4}
AlO_2^-	1.91×10^{-9}	3.89×10^{-8}	3.89×10^{-8}

Table 6. Mineral volume fraction (dimensionless, ratio of the volume for a mineral to the total volume of medium)

	FEBEX bentonite	Granite	Argillite
Calcite	0.00472	0	0.1
Smectite	0.546	0	0.1426
Chlorite	0.0024	0	0.1445
Quartz	0.012	0.3	0.1845
K-Feldspar	0.0059	0.35	0
Plagioclase	0	0.25	0
Mica	0	0.1	0
Dolomite	0.0	0	0

Illite	0.0001	0	0.223
Kaolinite	0.0	0	0.174
Siderite	0.0	0	0.01256
Ankerite	0.0	0	0.00798

2.3. Simulator

TOUGHREACT V3.3-OMP (Xu et al., 2014) is used to simulate the processes in the conceptual model. It is a major new release of TOUGHREACT (Xu et al., 2011) that includes many new features and parallelization of the most CPU-intensive calculations in reactive-transport model simulations. It can be applied to one-, two-, or three-dimensional porous and fractured media with physical and chemical heterogeneity, and can accommodate any number of chemical species present in liquid, gas, and solid phases. A variety of subsurface thermal, physical, chemical, and biological processes are considered in TOUGHREACT under a wide range of conditions of pressure, temperature, water saturation, ionic strength, pH, and Eh. The major chemical reactions include aqueous complexation, acid-base, redox, gas dissolution/exsolution, cation exchange, mineral dissolution/precipitation, and surface complexation.

The TOUGH2/EOS4 module is used for our multiphase flow calculation. TOUGH2 is a simulator based on the integral finite difference method, which offers the advantage of being applicable to regular or irregular discretization in one, two, and three dimensions (Pruess et al., 1999). Governing equations of TOUGH2 are established from mass and energy balance. The EOS4 module considers non-isothermal two phase (air and water) flow, with each individual phase flux given by a multiphase version of Darcy’s law. For vapor flow in the air phase, in addition to Darcy flow, mass transport can also occur via diffusion and dispersion according to Fick’s law. Thermal behavior is relatively well understood because it is less affected by coupled processes than by hydrological and chemical processes, and the relevant parameters can be reliably measured. Time is discretized fully implicitly as a first-order backward finite difference. The nonlinear equations in the residual form are solved by Newton/Raphson iteration.

3. Results of the Base Model

Models for Case_G and Case_A consider a waste package, a bentonite EBS, and a host rock. The models run for 100,000 years. It

is assumed that canisters are fully corroded and U(VI) is released by the dissolution of schoepite after 1000 years. Considering the large uncertainties associated with the process and parameters involved in a THC model of a repository, the model results in the paper are better viewed as one particular case; generalization of specific results should be done carefully**.** Note that the assumption that canister failure would occur in 1000 years is conservative. Choosing another time as the starting point for U(VI) might affect the comparison with other THC simulations regarding radionuclide migration, but probably not significantly. For example, De Windt et al. (2006) assumed that canister failure occurs after 10,000 years. However, after 1,000 years, the EBS becomes fully saturated and bentonite-host rock interactions are close to equilibrium conditions, THC processes evolve slowly thereafter. In other words, the THC environment in which radionuclides migrate would not change substantially from 1,000 years to 10,000 years. Therefore, it is expected that the starting time of U(VI) release, whether it is 1,000 years or 10,000 years, would not affect model results significantly.

3.1. TH evolution

The TH behaviors are described by the temperature, saturation, and pore pressure evolution around the repository at monitoring points A, B, C, and D, as marked in Fig. 1. A maximum temperature of about 100℃ is reached at the surface of the waste canister at ~5 years for both Case_A and Case_G. Temperature peaks later with the increase in the distance from the waste package. At the bentonite-host rock interface, the temperature summit is reached at about 25 years, and then the temperature declines steadily. After 1,000 years, the temperature falls to ~18℃ at these monitoring points at 100,000 years for both cases. Although the argillite of Case_A has lower thermal conductivity than the granite of Case_G, the computed temperature in both cases differs only moderately at early times.

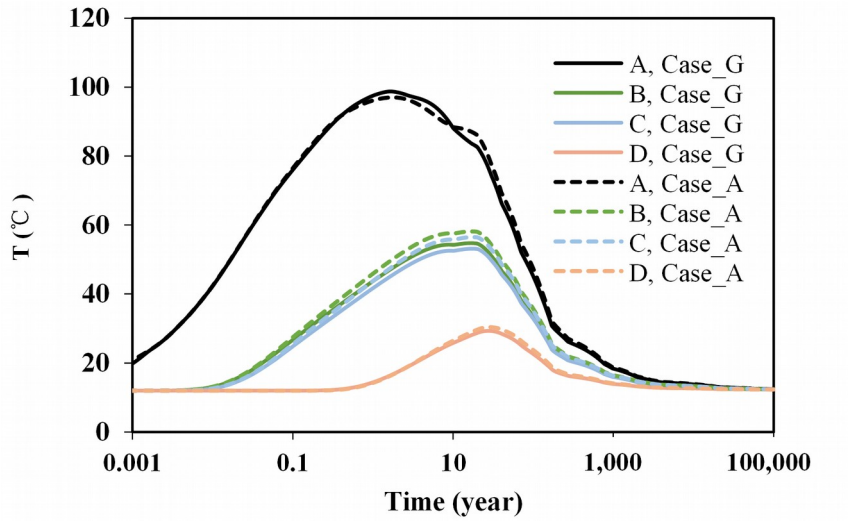

Fig. 2. Temporal evolution of temperature at points A, B, C, and D for Case_A and Case_G.

Because the host rock stays fully saturated (except in the area near the bentonite-host rock interface) for a very short time period, only the evolution of liquid saturation in bentonite (points A and B) in both cases are shown in Fig. 3. In the area close to the waste package (point A), bentonite undergoes desaturation first due to heating from the waste package and then gradually becomes fully saturated. In the vicinity of the bentonite-host rock interface (point B), bentonite becomes fully saturated in a relatively short time. Because (1) water infiltration into bentonite is determined predominantly by capillary pressure gradient (suction force) and (2) argillite has higher porosity than granite, bentonite is saturated at a faster rate in Case_A than in Case_G, despite granite having higher permeability than argillite.

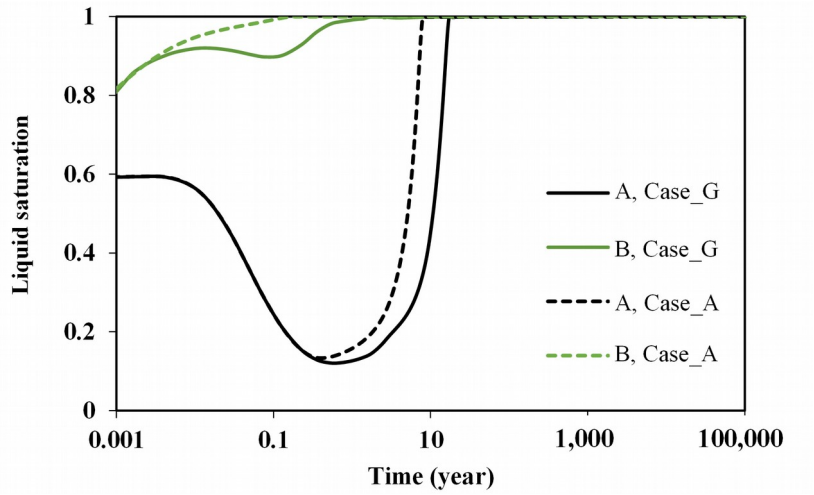

Fig. 3. Temporal evolution of liquid saturation at points A and B for Case_ A and Case_G.

Fig. 4 shows the evolution of pore pressure at A, B, C, and D in both cases. Regarding the pore pressure in bentonite in granite and argillite host rock, there are three noticeable differences: First, an increase in pore pressure in bentonite occurs earlier for Case_A than for Case_G. Second, the peak pore pressure in bentonite is higher in Case_A: the peak pore pressure reaches ~9 MPa in Case_A, which is 3 times higher than that in Case_G (2.88 MPa). Third, after the pore pressure in bentonite reaches steady state, it still maintains a relatively higher level in Case_A than in Case_G. For other points (B/C/D), whatever the host rock is, it tends to keep a constant pressure (0.63 MPa) over time.

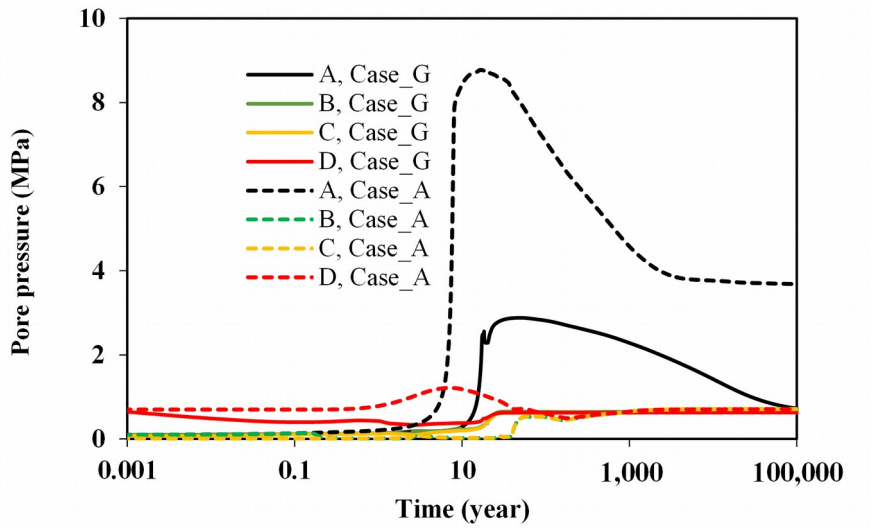

Fig. 4. Temporal evolution of pore pressure at monitoring points for Case_G and Case_A.

3.2. Geochemical evolution

As mentioned above, the model assumes that release of U(VI) won't occur until 1000 years. When U(VI) is released via dissolution of schoepite, the chemical conditions, especially within the bentonite barrier, play an important role because they affect the dissolution of schoepite and aqueous complexation with U(VI). As shown by some studies (e.g., Zheng et al., 2015), the interaction between host rock and bentonite barrier affects the geochemical evolution within the bentonite barrier. Similarly, we expect that Case_G leads to a different geochemical evolution within the bentonite barrier than Case_A.

The evolution of pH, and the concentration of Ca^{+2} and HCO_3^- , at points A and B are plotted in Fig. 5. The pH in the bentonite remains low for the first 10,000 years, due to the buffer created by surface

protonation reactions, and then increases from 10,000 to 30,000 years, and eventually plateaus until 100,000 years. The concentrations of Ca^{+2} and HCO_3^- are strongly affected by the dissolution of calcite and precipitation of dolomite, and fluctuate significantly when bentonite transitions from unsaturated to fully saturated.

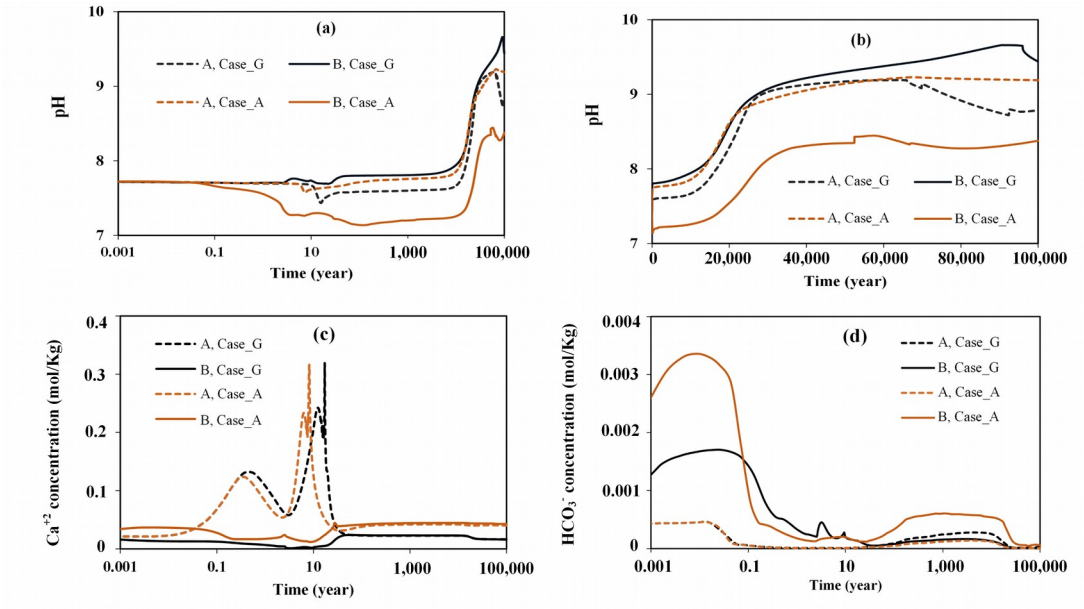

Fig. 5. Evolution of pH and concentration of Ca^{+2} and HCO_3^- at points A and B for Case_G and Case_A : (a) pH with logarithmic time, (b) pH with linear scale, (c) concentration of Ca^{+2} and (d) concentration of HCO_3^-.

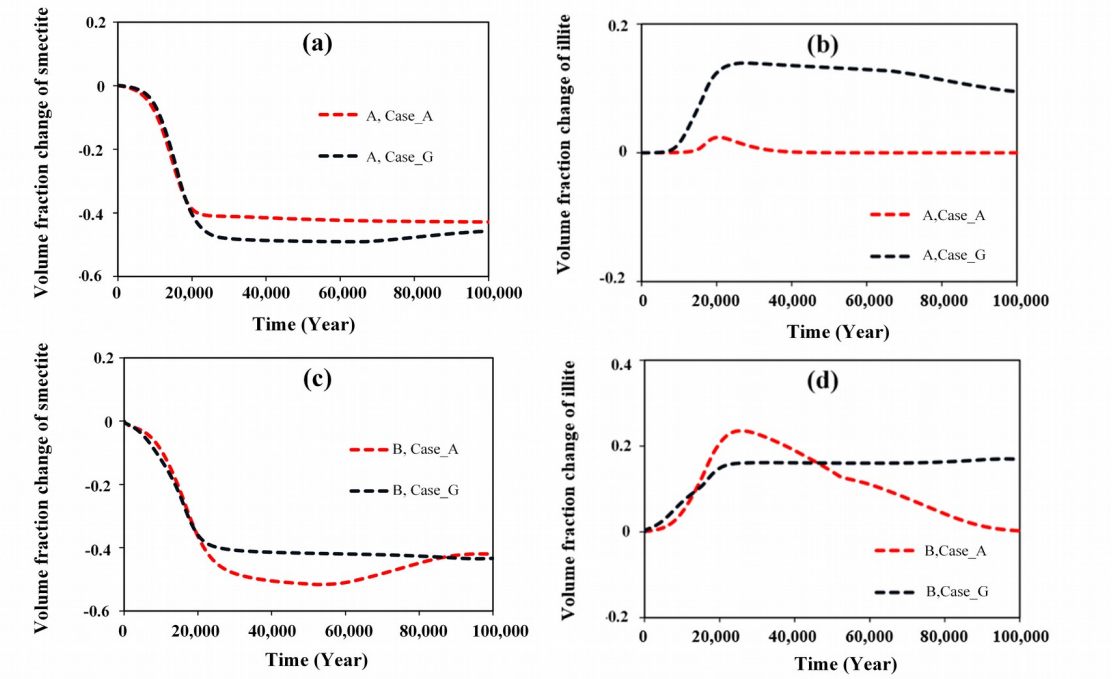

Fig. 6. Evolution of smectite and illite volume fraction at point A and B for Case_G and Case_A : (a) smectite volume fraction change at point A, (b) illite volume fraction change at point A, (c) smectite volume fraction change at point B, (d) illite volume fraction change at point B. Note negative value means dissolution and positive means precipitation.

In addition to the dissolution/precipitation of carbonate minerals, the most noticeable mineral phase change in bentonite is the dissolution of smectite and precipitation of illite (Fig. 6), a phenomenon known as illitization. Over the course of illitization, protons are consumed and pH increases (Fig. 5a). It is certainly not a surprise that when significant illitization occurs, roughly from 10,000 to 30,000 years (Fig. 6), pH increases as well (Fig. 5).

The chemical conditions in bentonite are controlled by the bentonite-host rock interaction under the influence of temperature and pressure change. Pore-water in argillite (Case_A) has lower pH and higher concentration of major ions than that in granite (Case_G), which is the primary reason for the different geochemical evolution in bentonite in Case_A and Case_G . For example, higher K concentration in argillite leads to higher K in bentonite and subsequently less illitization and lower pH in Case_A.

The dissolution of schoepite is influenced not only by the value of pH, but also by the concentration of Ca^{+2} and HCO_3^-, because the Ca-U-carbonate aqueous complexes are the dominant U (VI) aqueous species (Zheng et al., 2012). When the dissolution of schoepite occurs, the bentonite in Case_A has a lower pH, a higher concentration of Ca^{+2}, but a lower concentration of HCO_3^-, which affects the concentration of U(VI) at the source, i.e., waste package, as discussed in the following sections.

3.3. U(VI) migration

Fig. 7 shows the evolution of U(VI) at four monitoring points for both cases. Obviously, the concentrations at point A and B are very different when the host rock is different, which suggests that the host rock plays an important role in the migration of U(VI) in the bentonite barrier.

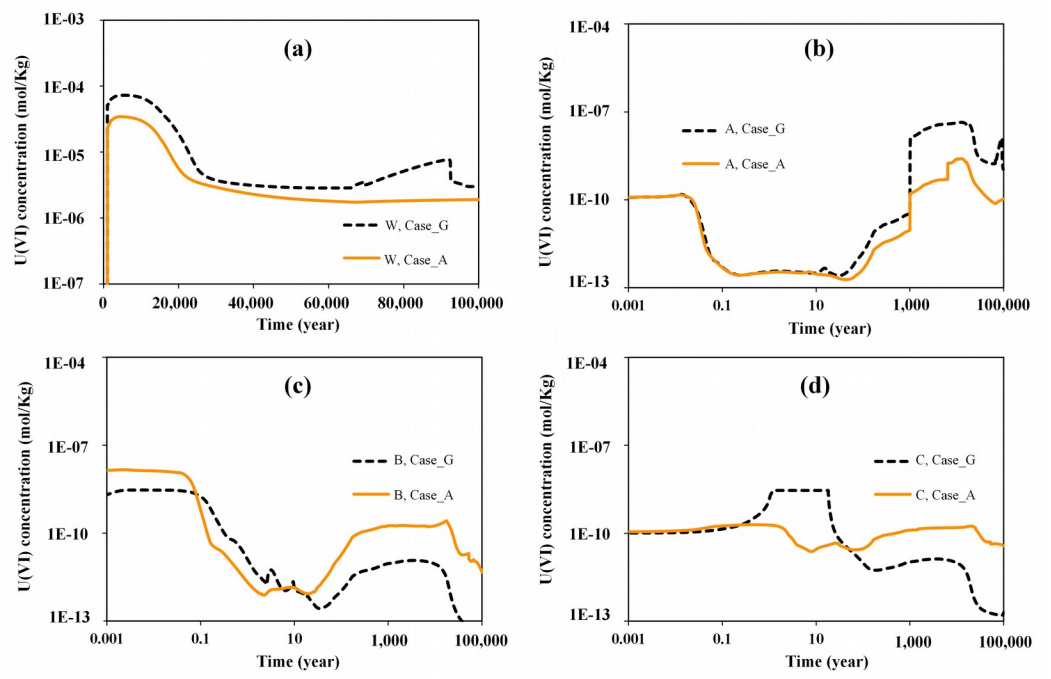

Fig. 7. Temporal evolution of U(VI) concentrations at waste package (a) and point A (b), B (c), C (d) in Case_G and Case_A.

Before the release of U(VI) from the waste package, i.e. from zero to 1000 years, the concentrations of U(VI) in bentonite (see points A and B) deviate from the initial concentrations due to variations in water saturation, reactions with exchangeable and sorption sites within bentonite, and interactions with host rock via diffusion.

When U(VI) is released from the waste package, the following reaction dominates:

Schoepite $+2Ca^{+2} + 3HCO_3^- = H^+ + 3H_2O + Ca_2UO_2(CO_3)_3$ (8)

which is a combination of reaction (2) and the dissociation of aqueous complex $Ca_2UO_2(CO_3)_3$. In the current model, $Ca_2UO_2(CO_3)_3$ and $CaUO_2(CO_3)_3^{-2}$ are the major aqueous species for U(VI). For example, shortly after 1000 years, at the waste package, $Ca_2UO_2(CO_3)_3$ accounts for 85.57% and $CaUO_2(CO_3)_3^{-2}$ for 13.69% of the total U(VI) concentration. The concentration of Ca^{+2}, HCO_3^- and pH affect the concentration of U(VI) (characterized by dominant $Ca_2UO_2(CO_3)_3$) through the ion activity product in the mass action law. The geochemical environment of bentonite in contact with the waste package for both host rocks are featured with slightly higher pH and Ca^{+2} concentration and lower HCO_3^- for Case_A compared to that for Case_G, which leads to higher total aqueous U(VI) concentration at the waste package for Case_G (Fig. 7, a).

When U(VI) starts to migrate through the bentonite after it is released from the waste package, a diffusion process and two surface-complexation reactions play the major role.

$$mon\_sOUO_2OH + 2Ca^{+2} + 3HCO_3^- = H_2O + H^+ + mon\_sOH + Ca_2UO_2(CO_3)_3 \quad (9)$$

$$mon\_sOUO_2(OH)_2^- + 2Ca^{+2} + 3HCO_3^- = 2H_2O + mon\_sOH + Ca_2UO_2(CO_3)_3 \quad (10)$$

Because the geochemical environment in bentonite for Case_A is characterized by slightly higher pH and Ca^{+2} concentration and lower HCO_3^- than that for Case_G, reactions (9) and (10) in bentonite are more favorable to the right-hand side for Case_A than for Case_G, which means less adsorption of U(VI) in bentonite for Case_A than for Case_G. Thus, clearly, for Case_A (with argillite host rock), the source concentration is lower than that for Case_G (with granite host rock) and there is less adsorption in bentonite for the case with argillite. The differences in U(VI) concentration in bentonite for two host rock cases are the consequence of two competing factors: (1) lower source concentration tends to drive the concentration of U(VI) in bentonite lower, whereas [2] lower adsorption in bentonite causes higher concentration in bentonite. These two factors are bridged by the diffusion processes: depending on the distance to the source, diffusion can help the effect of lower source concentration outperform the effect of lower adsorption, or vice versa. At point A, the concentration of total U(VI) concentration is lower for Case_A than Case_G (Fig. 7, b), because the concentration of U(VI) at the source is lower for Case_A, and point A is close to the source despite the lower adsorption in bentonite for Case_A. As we move further from the source, the source term plays a lesser role, and the lower adsorption in bentonite for Case_A makes the aqueous U(VI) higher for Case_A at points B and C (Fig. 7 c and d). Point D is too far from the source to show significant change in U(VI) concentration, and therefore model results for point D are not shown.

The dissolution of smectite and precipitation of illite leads to a rise in pH, which is balanced by carbonate minerals and causes a decrease in HCO_3^-. The net effect is that the dissolution of schoepite is inhibited, and U(VI) concentration at the source decreases (Fig. 7 a). As a result, U(VI) decreases temporally in bentonite for both host rock cases, as shown by decreasing concentrations over time at points A, B, and C. The decrease in HCO_3^- concentration drives even

stronger adsorption reactions, especially reaction (10), which leads to a strong adsorption of aqueous U(VI) and makes the aqueous U(VI) concentration even lower than the initial U(VI) concentration (See Fig. 7). In fact, the adsorption of U(VI) in bentonite is so strong that U(VI) is not able to migrate through the bentonite, and there is no increase in aqueous U(VI) concentrations in either host rock.

Table 7. The proportion of aqueous, exchanged, and adsorbed U(VI) to the total U(VI) mass for two host-rock cases (%).

Host rock	Monitoring point	Aqueous phase	Exchanged phase	adsorbed phase
Granite	A	0.0123	0.6915×10^{-7}	99.9877
	B	0.0168	0.2872×10^{-6}	99.9832
Argillite	A	0.0027	0.1354×10^{-7}	99.9973
	B	0.4779	0.1447×10^{-5}	99.5221

In the model, total U(VI) in bentonite is described as three phases: aqueous, exchanged, and adsorbed. Note that in most experimental work, exchanged and adsorbed phases are inseparable and usually treated as one phase. Table 7 shows the fraction of each phase relative to the total mass of U(VI) at points A and B for both host-rock cases. In both, the adsorbed phase is the dominant phase of U(VI), with a negligible exchange phase. The second is that the spatially, adsorbed phase accounts for more of the total U(VI) at locations close to the source (e.g., Point A) than locations far from the source (e.g., Point B). Obviously, less aqueous U(VI) is available for adsorption as U(VI) migrates away from the source.

In our current model, smectite and illite are the two adsorbents of U(VI). Roughly 80% of adsorbed U(VI) is on smectite by the end of the simulation time (Fig. 8). Although smectite dissolves and illite precipitates, there is still more smectite than illite in bentonite, and understandably that smectite is the major adsorbent. However, the proportion of U(VI) adsorbed on smectite varies spatially and temporally, largely following the evolution of smectite and illite.

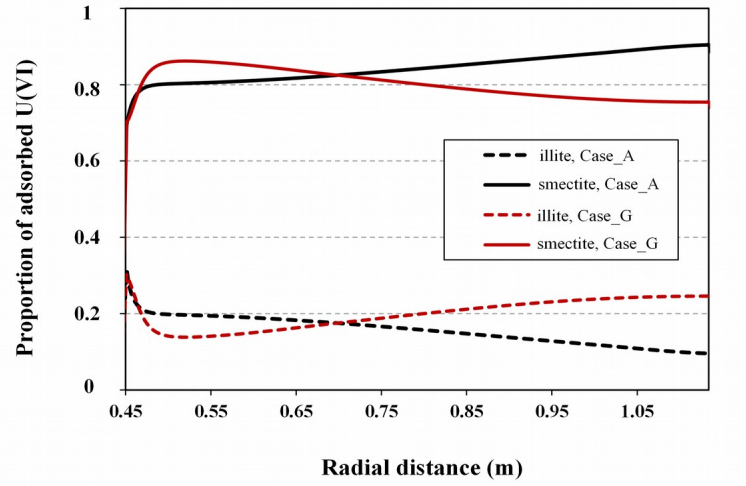

Fig. 8. Proportion of adsorbed U(VI) on smectite and illite: the sorption sites on smectite for Case_A (smectite, Case_A); the sorption sites on illite

for Case_A (illite, Case_A); the sorption sites on smectite for Case_G (smectite, Case_G); the sorption sites on illite for Case_G (illite, Case_G).

Our model shows that the bentonite barrier is very effective in retarding the migration of U(VI) released from the waste package. U(VI) concentration at point C for granite host rock is never above the background U(VI) concentration and lower than that for argillite host rock. In an EBS with bentonite, because of the bentonite-granite interaction, granite actually lead to a chemical condition in bentonite favorable to more adsorption of U(VI), and makes it a better host rock than argillite with respect to U(VI) migration, despite the fact that granite itself has very limited radionuclide-retarding capability compared with argillite.

4. A Sensitivity Analysis

As we discussed in the previous section, because of the high adsorption of bentonite, U(VI) does not appear in the host rocks, and therefore the difference between argillite and granite in terms of retarding the migration of U(VI) within host rocks cannot be compared. In addition, one might wonder how high the concentration of aqueous U(VI) in the host rock will be, or how far U(VI) travels in the host rock if bentonite has no adsorption capability. In this section, we therefore present a simulation in which all adsorption reactions (Table 1) for bentonite are disabled.

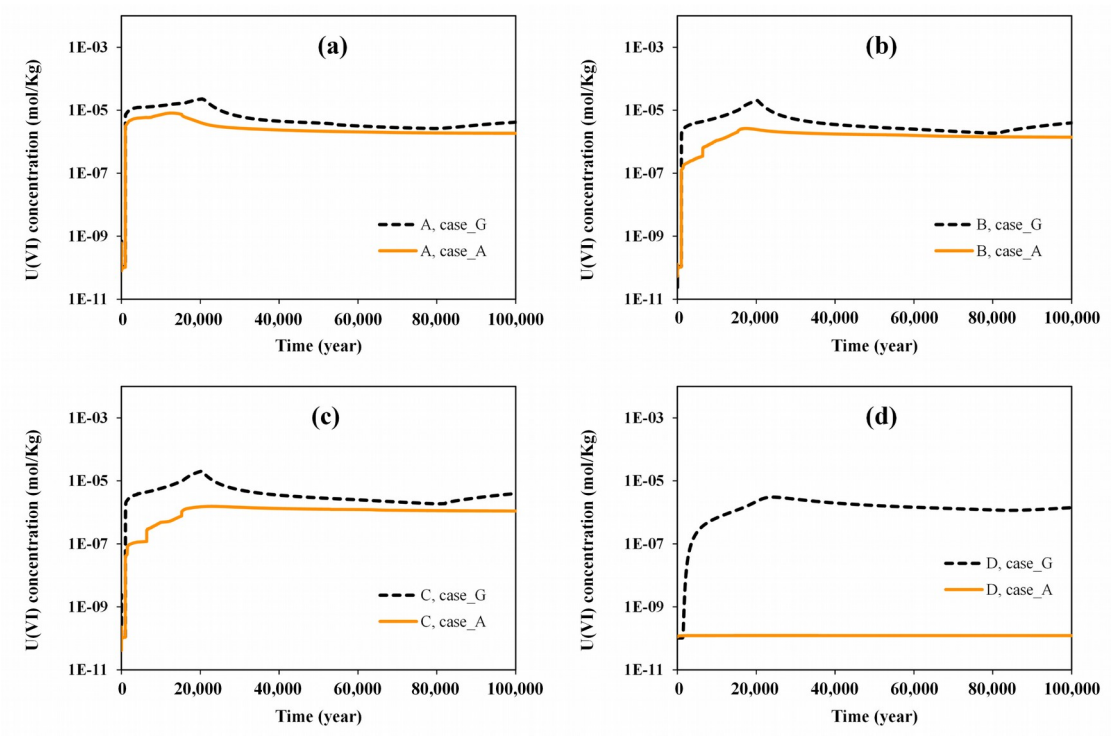

Fig. 9. Temporal evolution of the aqueous concentration of U(VI) at points A (a), B (b), C (c) and D (d) in the simulation that adsorption reactions in bentonite are disabled for Case_G and Case_A.

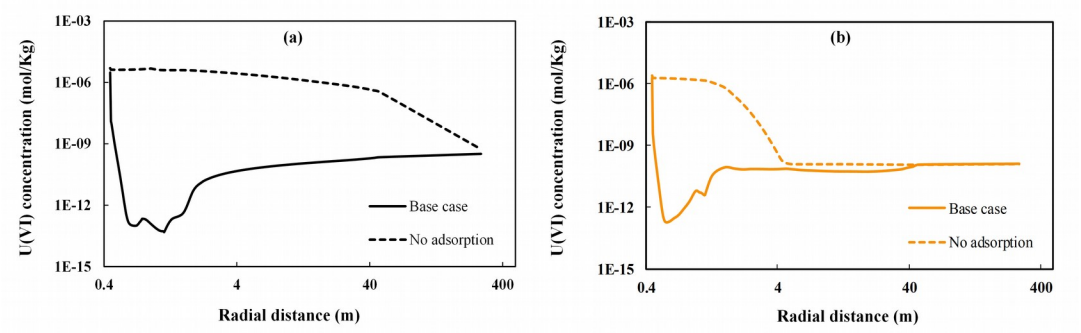

Fig. 10. Spatial aqueous concentration of U(VI) for the base model and a sensitivity run for Case_G (a) and Case_A (b) at 100,000 years, respectively.

As shown in Fig. 9, U(VI) concentration fluctuates near the background level in the first 1000 years. After U(VI) starts being released, the aqueous concentration of U(VI) quickly increases in the bentonite. Compared to the base model that considers adsorption in the bentonite (Fig. 7), the aqueous concentration of U(VI) is obviously higher in the sensitivity run that does not consider adsorption in bentonite. U(VI) migrates through the bentonite barrier and appears in host rock, as shown by the high U(VI) concentrations at points C and D. It takes only 3 years for aqueous U(VI) to migrate through the entire bentonite barrier. After that, the difference between argillite and granite in adsorption capability begins to manifest itself: U(VI) moves as deep as 275 m into the granite host rock in 100,000 years , whereas it travels only up to 4 m into the argillite host rock (Fig. 10), apparently because argillite has higher adsorption capability than granite. U(VI) penetrates to a lesser degree into the argillite, and the maximum aqueous concentration of U(VI) is also lower as well: the aqueous concentration of U(VI) at point C in argillite is one order of magnitude lower than that in granite.

5. Conclusion

HLW repositories hosted in (1) argillite and (2) granite are two disposal concepts that have been extensively studied. Among many measures to assess the performance of a repository, the migration of radionuclides within the repository is a critical one. Assuming they have the same engineered barrier system (EBS), how do different host rocks (argillite vs granite) affect the migration of U(VI)

in EBS bentonite and host rocks, and which properties of the host rock cause the difference? Here, we present coupled THC models with transport of U(VI) that have an identical setup except for the type of host rock (argillite vs granite rock). One model assumes that the host rock has the properties of granite from Beishan, China (Cao et al., 2017a); the other assumes that the host rock has properties of argillite from Opalinus Clay in Belgium (Bossart, 2011; Lauber et al., 2000). Both models assume an EBS with the properties of FEBEX bentonite (ENRESA, 2000). Thermal, hydrological, and chemical evolutions in the bentonite were examined for both cases, with a focus on the migration of U(VI). We make the following observations:

- Because water infiltration into bentonite from host rock is predominately controlled by the capillary pressure gradient, argillite host rock that has higher porosity actually leads to faster hydration of bentonite than granite, despite argillite having a lower permeability than granite.
- The chemical conditions within bentonite are controlled by the bentonite-host rock interaction under the influence of temperature and pressure. Different host rocks exert their influence on the migration of U(VI) via regulating the chemical conditions in the bentonite, which affect the concentration of U(VI) at the source and the adsorption of U(VI) in the bentonite.
- The key chemical conditions affecting the release and migration of U(VI) are pH, Ca^{+2}, and HCO_3^- concentrations in pore-water, which are strongly affected by the dissolution/precipitation of soluble carbonate minerals.
- Our model shows the occurrence of illitization (dissolution of smectite and precipitation of illite) in the bentonite, which affect the migration of U(VI) through changing pH and the quantity of adsorbents.
- Pore-water (groundwater) chemistry is the most important property of the host rock, affecting the migration in bentonite because of its influence on chemical conditions in the bentonite.
- For the particular hypothetical cases simulated in this paper, when there is an EBS filled with bentonite, granite actually leads to a chemical condition in bentonite more favorable to adsorption of U(VI), making it a better host rock than argillite with respect to U(VI) migration, despite granite itself having very limited retarding capability for radionuclides compared with argillite.

Although generalization of current model results for granite and

argillite should be done carefully, these simulations particularly highlight the importance of pore-water chemistry in host rock and bentonite-host rock interaction. And more importantly, when we think about repository, when there is bentonite backfill, the low sorption capacity of granite does not necessarily matter, and assuming it is disadvantageous for granite is not prudent. Compared to properties such as thermal conductivity, permeability, porosity and adsorption capacity, which have been commonly paid great attention, the pore-water chemistry of the host rock has been largely overlooked. But in fact it deserves equal or even more attention, because it most profoundly affects the migration of radionuclides.

Acknowledgements

This work was supported by the Spent Fuel and Waste Science and Technology Campaign, Office of Nuclear Energy, of the U.S. Department of Energy under Contract Number DE-AC02-05CH11231 with Lawrence Berkeley National Laboratory, and the Research and Development Project on the Geological Disposal of High Level Radioactive Waste by the State Administration of Science, Technology and Industry for National Defense under Grant Number: 2012–240. We would also like to thank the China Scholarship Council for their financial support.

References

Baeyens, B. et al., 2014. Sorption data bases for argillaceous rocks and bentonite for the provisional safety analyses for SGT-E2 (No. NTB--12-04). Paul Scherrer Institute (PSI).

Barnichon, J.-D., Volckaert, G., 2003. Observations and predictions of hydromechanical coupling effects in the Boom clay, Mol Underground Research Laboratory, Belgium. Hydrogeology Journal. 11, 193-202.

Bernot, P., 2005. Dissolved concentration limits of radioactive elements (No. ANL-WIS-MD-000010 REV 05). Yucca Mountain Project, Las Vegas, Nevada.

Bethke, C.M., Brady, P.V., 2010. How the Kd Approach Undermines Ground Water Cleanup. Ground Water. 38, 435-443.

Bianchi, M., H.-H., L., Birkholzer, J., 2013. Diffusion Modeling in a Clay Repository: FY13 Report (FCRD-UFD-2013-000228), Lawrence Berkeley National Laboratory, Berkeley.

Bianchi, M., Liu, H.H., Birkholzer, J.T., 2015. Radionuclide transport behavior in a generic geological radioactive waste repository. Groundwater. 53, 440-451.

Bossart, P., 2011. Characteristics of the Opalinus Clay at Mont Terri. Mont Terri Project, Wabern Switzerland.

Boult, K.A. et al., 1998. Towards an understanding of the sorption of U(VI) and Se(IV) on sodium bentonite. Journal of Contaminant Hydrology. 35, 141-150.

Bradbury, M.H., Baeyens, B., 2005. Modelling the sorption of Mn(II), Co(II), Ni(II), Zn(II), Cd(II), Eu(III), Am(III), Sn(IV), Th(IV), Np(V) and U(VI) on montmorillonite: Linear free energy relationships and estimates of surface binding constants for some selected heavy metals and actinides. Geochimica Et Cosmochimica Acta. 69, 875-892.

Bradbury, M.H., Baeyens, B., 2009a. Sorption modelling on illite Part I: Titration measurements and the sorption of Ni, Co, Eu and Sn. Geochimica Et Cosmochimica Acta. 73, 990-1003.

Bradbury, M.H., Baeyens, B., 2009b. Sorption modelling on illite. Part II: Actinide sorption and linear free energy relationships. Geochimica Et Cosmochimica Acta. 73, 1004-1013.

Bradbury, M.H., Baeyens, B., 2011. Predictive sorption modelling of Ni(II), Co(II), Eu(IIII), Th(IV) and U(VI) on MX-80 bentonite and Opalinus Clay: A “bottom-up” approach. Applied Clayence. 52, 27-33.

Bruno, J., Arcos, D., Cera, E., Duro, L., Grivé, M., 2004. Modelling near- and far-field processes in nuclear waste management. Geological Society London Special Publications. 236, 515-528.

Burkart, W., Danesi, P.R., Hendry, J.H., 2005. Properties, use and

health effects of depleted uranium. International Congress. 1276, 133-136.
Cao, X., Hu, L., Wang, J., Wang, J., 2017a. Radionuclide transport model for risk evaluation of high-level radioactive waste in Northwestern China. Human and Ecological Risk Assessment: An International Journal. 23, 2017-2032.
Cao, X., Hu, L., Wang, J., Wang, J., 2017b. Regional Groundwater Flow Assessment in a Prospective High-Level Radioactive Waste Repository of China. Water. 9, 551.
Chen, Y., Zhou, C., Jing, L., 2009. Modeling coupled THM processes of geological porous media with multiphase flow: theory and validation against laboratory and field scale experiments. Computers and Geotechnics. 36, 1308-1329.
Chung, K.-w., Chul-Joo, K., Yoon, H.-S., 2013. Uranium ion exchange adsorption method using ultrasound. Google Patents.
Davis, J.A., Coston, J.A., Kent, D.B., Fuller, C.C., 1998. Application of the Surface Complexation Concept to Complex Mineral Assemblages. Environmental Science & Technology. 32, 2820-2828.
Davis, J.A., Meece, D.E., Kohler, M., Curtis, G.P., 2004. Approaches to surface complexation modeling of Uranium(VI) adsorption on aquifer sediments 1. Geochim.cosmochim.acta. 68, 3621-3641.
De Windt, L., Burnol, A., Montarnal, P., Van Der Lee, J., 2003. Intercomparison of reactive transport models applied to UO2 oxidative dissolution and uranium migration. Journal of contaminant hydrology. 61, 303-312.
De Windt, L. et al., 2006. Modeling spent nuclear fuel alteration and radionuclide migration in disposal conditions. Radiochimica Acta. 94, 787-794.
Dong, W.; Brooks, S. C., Determination of the Formation Constants of Ternary Complexes of Uranyl and Carbonate with Alkaline Earth Metals (Mg2+, Ca2+, Sr2+, and Ba2+) Using Anion Exchange Method. Environ. Sci. Technol. 2006, 40, (15), 4689-4695.
Fernández, A.M., Cuevas, J., Rivas, P., 2000. Pore-water chemistry of the FEBEX bentonite. MRS Online Proceedings Library Archive, 663.
Fernández, A.M.A., Baeyens, B., Bradbury, M., Rivas, P., 2004. Analysis of the porewater chemical composition of a Spanish compacted bentonite used in an engineered barrier. Physics & Chemistry of the Earth. 29, 105-118.
Fernández, A.M.A. et al., 2007. On site measurements of the redox and carbonate system parameters in the low-permeability Opalinus Clay formation at the Mont Terri Rock Laboratory. Physics & Chemistry of the Earth. 32, 181-195.

Fouché, O., Wright, H., Le Cléac'h, J.-M., Pellenard, P., 2004. Fabric control on strain and rupture of heterogeneous shale samples by using a non-conventional mechanical test. Applied Clay Science. 26, 367-387.

Fox, P. M.; Davis, J. A.; Zachara, J. M., The effect of calcium on aqueous uranium(VI) speciation and adsorption to ferrihydrite and quartz. Geochim. Cosmochim. Acta 2006, 70, (Journal Article), 1379-1387.

Gao, X., Bi, M., Shi, K., Wu, W., Chai, Z., 2017. Sorption characteristic of uranium(VI) ion onto K-feldspar. Appl Radiat Isot. 128, 311-317.

Gens, A., Guimaräes, L.d.N., Olivella, S., Sánchez, M., 2010. Modelling thermo-hydro-mechano-chemical interactions for nuclear waste disposal. Journal of Rock Mechanics and Geotechnical Engineering. 2, 97-102.

Gens, A. et al., 2009. A full-scale in situ heating test for high-level nuclear waste disposal: observations, analysis and interpretation. Géotechnique. 59, 377-399.

Greenberg, H., Blink, J., Buscheck, T., 2013. Repository Layout and Required Ventilation Trade Studies in Clay/Shale using the DSEF Thermal Analytical Model (No. LLNL-TR-638880). Lawrence Livermore National Lab.(LLNL), Livermore, CA (United States).

Hadermann, J., Heer, W., 1996. The Grimsel (Switzerland) migration experiment: integrating field experiments, laboratory investigations and modelling. Journal of Contaminant Hydrology. 21, 87-100.

Hansen, F.D. et al., 2010. Shale disposal of US high-level radioactive waste, SAND2010-2843, Sandia National Laboratories, SANDIA.

Hardin, E. et al., 2015. Investigations of Dual-Purpose Canister Direct Disposal Feasibility (No. SAND2015-1804C), Sandia National Lab, Albuquerque, NM (United States).

Ho, C.K., Webb, S.W., 1996. A review of porous media enhanced vapor-phase diffusion mechanisms, models, and data: Does enhanced vapor-phase diffusion exist? Journal of Porous Media. 1, 71-92.

Huertas, F. et al., 2000. Full-scale engineered barriers experiment for a deep geological repository for high-level radioactive waste in crystalline host rock(FEBEX project). EUR(Luxembourg).

Jin, Q. et al., 2016. Surface complexation modeling of U (VI) adsorption on granite at ambient/elevated temperature: experimental and XPS study. Chemical Geology. 433, 81-91.

JNC, H., 1999. Project to Establish the Scientific and Technical Basis for HLW Disposal in Japan, Supporting Report I, Geological Environment in Japan, pp, III-119-III-120.

Joseph, C. et al., 2017. Long-term diffusion of U(VI) in bentonite:

Dependence on density. Science of the Total Environment. 575, 207-218.
Kuhlman, U., Gaus, I., 2014. THM Model validation modelling of selected WP2 experiments: Inverse Modelling of the FEBEX in situ test using iTOUGH2. DELIVERABLE.
Lauber, M., Baeyens, B., Bradbury, M.H., 2000. Physico-Chemical Characterisation and Sorption Measurements of Cs, Sr, Ni, Eu, Th, Sn and Se on Opalinus Clay from Mont Terri (No. PSI--00-10), Paul Scherrer Inst.
Li, X., 2017. Partical mechanics modeling of thermal effects on shear behavior of granitic fracture rocks in Beishan, Gansu Province, China university of geosciences (Beijing).
Lin, Q. et al., 2009. Time-dependent strength degradation of granite. International Journal of Rock Mechanics and Mining Sciences. 46, 1103-1114.
Lubchenko, N. et al., 2015. Modeling of the Groundwater Transport Around a Deep Borehole Nuclear Waste Repository (No. INL/CON-15-34979), Idaho National Lab.(INL), Idaho Falls, ID (United States).
Majdan, M. et al., 2010. Characterization of uranium(VI) sorption by organobentonite. Applied Surface Science. 256, 5416-5421.
Martin, C., Christiansson, R., 2009. Estimating the potential for spalling around a deep nuclear waste repository in crystalline rock. International Journal of Rock Mechanics and Mining Sciences. 46, 219-228.
Meier, P., Trick, T., Blümling, P., Volckaert, G., 2000. Self-healing of fractures within the EDZ at the Mont Terri Rock Laboratory: results after one year of experimental work, Proceedings of international workshop on geomechanics, hydromechanical and thermohydro-mechanical behaviour of deep argillaceous rocks: Theory and experiment. Swets & Zeitlinger. 2000, 267-274.
Missana, T., GarcíA-Gutiérrez, M., Alonso, Ú., 2004. Kinetics and irreversibility of cesium and uranium sorption onto bentonite colloids in a deep granitic environment. Applied Clay Science. 26, 137-150.
Oecd, 2006. Physics and Safety of Transmutation Systems: A Status Report. Oecd Papers. 6, 13-13.
Patriarche, D., Ledoux, E., Simon-Coinçon, R., Michelot, J.-L., Cabrera, J., 2004. Characterization and modeling of diffusion process for mass transport through the Tournemire argillites (Aveyron, France). Applied clay science. 26, 109-122.
Pruess, K., Oldenburg, C.M., Moridis, G.J., 1999. TOUGH2 User's Guide Version 2. Office of Scientific & Technical Information Technical Reports.

RamíRez, S., Cuevas, J., Vigil, R., Leguey, S., 2002. Hydrothermal alteration of “La Serrata” bentonite (Almeria, Spain) by alkaline solutions. Applied Clay Science. 21, 257-269.

Reinoso-Maset, E., Ly, J., 2016. Study of uranium(VI) and radium(II) sorption at trace level on kaolinite using a multisite ion exchange model. J Environ Radioact. 157, 136-148.

Rutqvist, J., Zheng, L., Chen, F., Liu, H.-H., Birkholzer, J., 2014. Modeling of coupled thermo-hydro-mechanical processes with links to geochemistry associated with bentonite-backfilled repository tunnels in clay formations. Rock Mechanics and Rock Engineering. 47, 167-186.

Sánchez, M., Gens, A., Olivella, S., 2012. THM analysis of a large-scale heating test incorporating material fabric changes. International Journal for Numerical and Analytical Methods in Geomechanics. 36, 391-421.

SKB, 2006. Long-term safety for SKB-3 repositories at Forsmark and Laxemar — a first evaluation. , Main report of the SR-Can project.

Spycher, N.F. et al., 2011. Biogenic uraninite precipitation and its reoxidation by iron (III)(hydr) oxides: A reaction modeling approach. Geochimica et Cosmochimica Acta. 75, 4426-4440.

Stewart, B. D.; Mayes, M. A.; Fendorf, S., Impact of Uranyl−Calcium−Carbonato Complexes on Uranium(VI) Adsorption to Synthetic and Natural Sediments. Environ. Sci. Technol. 2010, 44, (3), 928-934.

Tournassat, C.; Tinnacher, R. M.; Grangeon, S.; Davis, J. A., Modeling uranium(VI) adsorption onto montmorillonite under varying carbonate concentrations: A surface complexation model accounting for the spillover effect on surface potential. Geochim. Cosmochim. Acta 2018, 220, (Supplement C), 291-308.

Vomvoris, S., Birkholzer, J., Zheng, L., Gays, I., Blechschmidt, I., 2015. THMC behavior of claybased barriers under high temperature–from laboratory to URL scale, Proceedings, International High-Level Radioactive Waste Management Conference, Charleston, NC, USA.

Voutilainen, M. et al., 2017. Modeling transport of cesium in Grimsel granodiorite with micrometer scale heterogeneities and dynamic update of Kd. Water Resources Research. 53, 9245-9265.

Wei, H.G., 2012. Investigation of sorption and migration effect factors of uranium on granites in Beishan. Geoscience. 26, 823-828.

Wronkiewicz, D.J., Bates, J.K., Wolf, S.F., Buck, E.C., 1996. Ten-year results from unsaturated drip tests with UO2 at 90 C: implications for the corrosion of spent nuclear fuel. Journal of Nuclear Materials. 238, 78-95.

Xu, T., Sonnenthal, E., Spycher, N., Zheng, L., 2014. TOUGHREACT V3. 0-OMP reference manual: a parallel simulation program for non-isothermal multiphase geochemical reactive transport. University of California, Berkeley.

Xu, T. et al., 2011. TOUGHREACT Version 2.0: A simulator for subsurface reactive transport under non-isothermal multiphase flow conditions. Computers & Geosciences. 37, 763-774.

Zheng, L., Kim, K., Xu, H., Rutqvist, J., 2016. DR Argillite Disposal R&D at LBNL (No. LBNL-1006013). Lawrence Berkeley National Lab.(LBNL), Berkeley, CA (United States).

Zheng, L., Rutqvist, J., Birkholzer, J.T., Liu, H.-H., 2015. On the impact of temperatures up to 200 C in clay repositories with bentonite engineer barrier systems: A study with coupled thermal, hydrological, chemical, and mechanical modeling. Engineering Geology. 197, 278-295.

Zheng, L. et al., 2014. Investigation of Coupled Processes and Impact of High Temperature Limits in Argillite Rock (No. LBNL-6719E). Lawrence Berkeley National Lab.(LBNL), Berkeley, CA (United States).

Zheng, L., Samper, J., 2008. A coupled THMC model of FEBEX mock-up test. Physics and Chemistry of the Earth, Parts A/B/C. 33, S486-S498.

Zheng, L., Samper, J., Montenegro, L., 2011. A coupled THC model of the FEBEX in situ test with bentonite swelling and chemical and thermal osmosis. Journal of contaminant hydrology. 126, 45-60.